THE APPLICATION OF AIRBORNE AND SATELLITE SAR
TO SEA ICE GEOPHYSICAL INVESTIGATIONS

Mark R. Drinkwater
Jet Propulsion Laboratory
California institute of Technology
4800 Oak Grove Drive
Pasacicna CA 91109

1. INTRODUCTION

2. SAR AND THE STUDY OF SEA ICE

    A. Scales of Surface Processes in Space and Time
    B. Characteristics of Operational SAR

        Satellite SAR
        Airborne SAR

    c. Seasat to the Present Day
    D. ERS-1 Validation Experiments

3. SPATIAL AND TEMPORAL RESOLUTION VS COVERAGE

    A. Spatial and Temporal Resolution
    B. Spatial Coverage

4. CM-WAVELENGTHS AND SEA ICE GEOPHYSICS

    A. impact of Frequency

        Microwave Signatures of Ice Types
        Transmission and Absorption of Microwaves

    B. Polarization Diversity

        Scattering model development
        Distinguishing between water and ice
        Resolving Ambiguities in Sea-Ice Classification

    c. Snowcover: A thermal insulator and microwave blanket
    D. Ice-Type Signatures
    E. Seasonal Impact
    F. Validation Measurements and Surface Proof

5. COUPLED DATA AND MODEL APPROACHES

    A. Microwave Scattering Models and Inversion
    B. Wind-Driven Ice Motion and the Momentum Balance
    c. SAR and Ice-ocean Model Surface Flux Estimates
        Coupling SAR Observations and Ice Growth Models
        Time-Series Backscatter Data and the Energy Budget

6, DISCUSSION AND CONCLUSIONS

1. INTRODUCTION

The logistical difficulties of making regular oceanographic measurements in the polar oceans during winter make it necessary to employ remote-sensing techniques. Microwave synthetic aperture radar (SAR) offers day and night imaging, without impact from atmospheric conditions. SAR satellite receiving stations located in Fairbanks, Alaska; Tromsø, Norway; Kiruna, Sweden; West Freugh, Scotland; and Gatineau, Canada, form a chain of station receiving masks which cover all but the Eastern Arctic basin. Similar SAR-satellite data receiving stations in the Antarctic are operated by the Germans at the Chilean General Bernardo O'Higgins base; and by the Japanese at the S yowa base [1]. A further receiving station is proposed and currently being implemented at the U.S. McMurdo base [2], to be operational in 1995-96, and will complete coverage of the Southern Ocean around the Antarctic continent. This network forms the basis for over a decade of continuous satellite SAR observations' of the polar ice pack in both hemispheres.

Sea ice plays a key role in climate through its interactions with and feedback's to the atmosphere and ocean [3]. As the extent of the sea ice is on average of the order of 10% of the global ocean area (rising to a maximum of 13%) this high albedo insulating layer acts as an intermediary in the way in which the local atmosphere communicates with the ocean. The sea-ice cover both reflects and responds to the balance of fluxes of momentum, heat, water vapour and salt at the surface, changing its distribution, thickness and salinity accordingly. Through the surface albedo and coverage of leads, the surface conditions of the sea ice impact the net heat flux at the surface and therefore the equilibrium thickness of the ice. Similarly, the winter sea-ice cover acts to precondition the mixed layer, due to salinization by salt rejection during sea-ice growth [4]. It has an effect on global ocean characteristics from the perspective of generation of water masses such as Antarctic bottom water or the high salinity shelf water found along the shelves of the Weddell and Ross Seas [5] and in the Beaufort and Chukchi Seas. Thus sea ice has an important impact beyond locally regulating the exchange of heat, momentum and water vapour between ocean and atmosphere.

in recent years SAR evolved and matured as an operational tool [6], but the data have barely been exploited to their full scientific potential. This chapter points toward some of the new insight SAR can give to polar oceanography, while identifying drawbacks and difficulties with SAR sea ice data and their application in geophysical investigations,

2. SAR AND T] IE STUDY OF SEA ICE

The conventional concern of high latitude oceanographers is that information gathered from space can not be as accurate or as relevant as that collected first hand from research vessels or *in-situ* by moorings or drifters. 1 lowever, microwave radar imaging of sea ice is a young and continuousl y evolving field, just as acoustic tomography and acoustic Doppler current profiling

once were. Synthetic Aperture Radar (SAR) remote sensing is the ideal candidate for monitoring sea ice characteristics at a variety of time and spatial scales. Currently operating satellites ERS-1 and J-ERS- 1, and operational airborne radar sensors will be succeeded for at least another decade, by operational SAR aboard ERS-2, Radarsat and the ESA Envisat Satellite. This will provide over 10 years of continuous and almost unrestricted high-resolution imaging.

A.   Scales of Surface Processes in Space and Time

The main problem in observing the polar ice cover and its influence on the atmospheric and oceanic boundary layer is the ephemerality of the active processes. Identifying the timescales of ice formation, change and decay, is the key to successful satellite monitoring of these processes. Sea ice continuously interacts with the ocean and atmosphere, and the spatial and temporal scales of these interactions respond to similar scales in the atmospheric and oceanographic forcing terms, ranging spatially from meters to thousands of kilometers, and temporally from diurnal to decadal. Table 1 indicates the spatial and temporal scales of key sea-ice variables of interest to sea-ice geophysicists and oceanographers.

Traditionally sea-ice extent ('l-able I.) is regarded as the parameter which microwave techniques can most successfully measure. This task is routinely accomplished by passive microwave instruments such as SSM/I which frequently map large areas (see Comiso, Chapt 5 Section aii). The additional capability which higher resolution techniques (ea. 30 m) such as SAR offer is that individual features of the sea-ice cover such as ice floes and leads can be monitored by tracking them in time-sequential images. Holt et al. [7] review this capability, demonstrating the ability of the instrument on board ERS- 1 to monitor the patterns of ice motion and circulation in the Arctic basin. Tools to obtain ice motion from spaceborne SAR images are adequate to make routine intensive observations in areas such as the Fram, Denmark, and the Bering Straits, Whereas ice motion in these areas is too vigorous for buoys to be efficient or cost-effective, SAR images can provide firm new data on the Arctic freshwater balance from measuring the ice mass flux through these regions. Equally important is the contribution of SAR to observing dynamics of leads and thin ice areas, lee-motion data generated from pairs of images separated at intervals of several days enable studies of the changes in thin ice area in relation to the motion field and spatial variations ice velocity. As subsequent sections will show, when this information is coupled with physical models of ice growth and air temperature and wind data, observations of divergence and thin ice formation in leads and polynyas can be employed in estimates of the brine flux or salt precipitation rate in the upper ocean. Models can be exploited to estimate the sensible and latent heat fluxes, and with sufficient coverage and frequency, enable regional heat budgets to be monitored. It is clear, therefore, that with combination of these data and information from judiciously placed buoys, SAR will be able to make significant contributions to acquiring information on the variables listed in Table 1.

B.   The Characteristics of Operational SAR

Knowledge of the specifications of operational SAR is important to the interpretation of acquired image data. Varying viewing geometry, frequency and polarization make it necessary to interpret the resulting microwave data with care. Equally important is the scale and frequency of coverage in relation to the processes identified in Table 11.

Satellite SAR

Past, present, and future SAR instruments arc described in 'l'able 11 for a comparison of their operating characteristics. Of the spaceborne SAR'S not listed, the Space Shuttle payload instrument called the Shuttle imaging Radar (SIR) recovered limited imagery of marginal ice in the Southern Ocean during the SIR-B mission in 1984 [8] and is not considered, Its follow-on SIR-C, slated for launch in 1994, will also have low orbit inclination and is excluded. Of the missions listed, ERS- 1 and J-Ill< S- 1 are currently flying, and recovering considerable amounts of data. Further information about the overall timetable for microwave instruments collecting sea-icc data is given in Carsey et al. [6] while the characteristics of each these instruments are described in detail by Massom [9].

Airborne SAR

Prom Seasat and the present day, airborne systems were the only means of developing capability to interpret microwave images of sca ice and laid valuable groundwork for present-day SAR systems. Until 1991, for instance, there was no spaceborne C-band microwave SAR. Several operational airborne science instruments acquired a wealth of data in preparation and support of satellite missions. The major characteristics of three notable systems arc outlined below to indicate the breadth of data characteristics. Only those systems participating in sea-ice experiments are listed. The CCRS, ERIM and JPL airborne instruments allowed collection of such data over the Barents, Beaufort, Bering, Chukchi, Greenland and I.abrader Seas during a variety of experiments.

CCRS Aircraft SAR
The Canada Centre for Remote Sensing (CCRS) airborne SAR is a 2 frequency C- (5.3 GHz: $\lambda =$ 5.66 cm) and X-band (9.6 GHz: $\lambda = 3.1$ cm) instrument which can operate in a number of imaging modes [10, 11]. These modes arc; (a) **Nadir** Mode - with an incidence angle range $0° < \theta < 74°$, a range and azimuth pixel resolution of approximately 6 m, and a swath width of 22 km ; (b) **Narrow Swath Mode** - with incidence angles from $45° < 0 < 76°$ a range and azimuth pixel resolution of approximately 6 m and a swath width of 18 km; (c) Wide Swath Mode - with an incidence angle range $45° < 0 < 85°$, a range and azimuth pixel resolution of approximately 20 m x 10 m and a swath width of 63 km. The radar can transmit and receive at both combinations of

linear horizontal and vertical polarization, enabling like- and cross-polarized images to be recorded, 'he system is flown aboard a Convair 580 twin-turboprop aircraft which has a flight range of about 2,500 km and endurance of 4.5 hours.

JPL AIRSAR

The NASA-JPL aircraft SAR (AIRSAR), is a 3-frequency synthetic aperture radar operating at P-band (0.44 GHz: λ = 68 cm); L-band (1.23 GHz: λ = 24 cm); and C-band (5.3 GHz: λ = 5.6 cm), The radar is fully polarimetric thereby offering a linear quad-polarized (hh, hv, vv, vh) amplitude and phase dataset which can be used to synthesize images any given transmit or receive polarization combination. This instrument is flown aboard a long-range DC-8@ aircraft which can carry other instrumentation in support of the radar. It has an operating range of approximately 3,200 km and a continuous operating time of 8 hours when flying the AIRSAR.

ERIM/NADC SAR

The Environmental Research Institute of Michigan/Naval Air Development Centre (ERIM)/NADC 3-frequency SAR is flown aboard a P-3 aircraft. This L- (1.2 GHz), C- (5.3 GHz), X-band (9.4 GHz) system is fully polarimetric, and has a resolution of about 1.8 m, in the incidence angle range 20° to 70°, over a swath of 10 km [12].

C. Seasat to the Present Day

In 1978 Seasat laid the foundations for SAR remote sensing of sea ice, returning high quality SAR images of the Beaufort and Chukchi ice pack before abruptly failing [13]. This short-lived mission of 105 days in orbit unfortunately precluded planned simultaneous surface measurement and validation experiments to understand the impact of sea-ice geophysics upon the L-band backscatter images. Since 1978, aircraft SAR and surface-based scatterometer measurements have been the mainstay for development in our understanding of the fundamentals of microwave interactions with snow and sea ice. in the interim period between Seasat and ERS- 1, the flexibility of airborne platforms enabled the continuing development of SAR applications in sea ice geophysics. A number of flight campaigns were conducted during field experiments where intensive surface measurements were made. Thus, until 1991 the only sea-ice surface measurements conducted simultaneous to SAR were during airborne campaigns.

One of the most intensive yet extended applications of airborne SAR has been throughout a series of experiments to study air-sea-interaction in the seasonal ice zone. Johannessen et al. [14] describe results of 1979 Norwegian Remote Sensing Experiment (NORSEX); the Marginal Ice Zone Experiments (MIZEX) conducted in 1983, 1984 and 1987 ; and the Seasonal Ice Zone Experiment (SIZEX) in 1989, These experiments employed early versions of the JPI. airborne SAR, the CCRS/ERIM SAR, and the CCRS radar described above. This series of experiments defined the role of SAR in monitoring the morphology and structure of the ice edge in the

5

Greenland Sea, Fram Strait and Barents Sea regions with application to monitoring mesoscale oceanographic activity and sea-ice dynamics along ice edges. Such SAR observations led to considerable interest in modeling ocean processes such as ice edge upwelling, eddy formation (see [14]) and deep convection[15] - all of which directly result in surface expressions traced by the SAR-imaged sea-ice drift.

in parallel to those described above, similar seasonal ice zone experiments were being conducted in the Labrador Sea in preparation for the use of C-band ERS- 1 and Radar sat data. The Labrader Ice Margin Experiments (LIMEX) were conducted in 1987 and 1989 with support from the CCRS airborne SAR carrying the first C-band airborne SAR [16, 17, 18, 19]. These experiments were unique in that they were the first to be conducted with an airborne C-band sensor. Results have led to developments in the understanding of wave imaging in marginal ice zones, the evaluation of C-band backscatter models for sea ice and the expression of different ice theologies upon marginal ice zone dynamics (for results see [20]).

Final mention must be made of a number of more recent preparatory experiments for utilization of ERS- 1 data in sea-ice monitoring. The first was the Bothnian Experiment in Preparation for ERS- 1 (BEPERS-88) taking place in the Gulf of Bothnia in February 1988 (see collection of papers in [21]). In the following year a series of experiments began in the Canadian archipelago. The Seasonal Ice Monitoring Site (SIMS) experiment was first conducted in Resolute Passage in May and June 1990 [22]. Continuation experiments have subsequently been conducted in 1991 and 1992 with the CCRS SAR to monitor seasonal change in Lancaster Sound, The latter was conducted under the new name Seasonal Ice Monitoring and Modelling Site (SIMMS '92). This new name reflects the evolution of this annual experiment towards utilizing time-series SAR and field data to model the snow and sea-ice response to short and long-wave radiation dynamics [23].

D.   ERS - 1 Validation Experiments

After failure to capture simultaneous field measurements during the Seasat mission, various experiments were conceived with the object of calibration of the radar or validating approaches to extract sea-ice information from ERS-1 SAR data during the early lifetime of the satellite. These were: ARCTIC '91, conducted in the late summer-early fall period in the high Arctic; the Baltic Experiment for ERS-1(BEERS-92) during January-March 1992 in the Gulf of Bothnia; the Seasonal Ice Zone Experiment (SIZEX-92) in the Barents Sea in March 1992; and the Winter Weddell Gyre Study (WWGS '92) in the Weddell Sea, Antarctica, from May - August 1992.

It is impossible to report on the preliminary findings of all of these individual studies, and so the reader is referred to papers presented about each of these individual experiments at the 1 irst ERS-1 Results Symposium, held at Cannes in November 1992 [24].

Validation activities have been focused on the capability of SAR to image, differentiate and monitor different types of sea ice. For the most part ERS-1 data is shown applicable to the problem of calculating areal fractions of different ice types, and especially to calculating the regional fraction of multiyear ice in the Arctic. Perhaps the most promising validation result is that SAR images can be used effectively to track ice floes under different conditions. Ice tracking opens many doors to future scientific investigations using these data, as kinematic information hold the key to estimating ice divergence and convergence, and therefore estimates of the thin ice fraction, the heat and salt fluxes into the upper ocean, and thus the ice growth rate. However, physical models must go hand-in-hand with the development of scientific applications of these data. Since the modeling community will be involved, it is necessary to point out drawbacks associated with utilizing SAR data.

3. SPATIAL AND TEMPORAL RE SOLUTION" VS COVERAGE

Experiments described in the previous section have provided a wealth of microwave signature data accessible to scientists. image data acquired in conjunction with surface measurements provide the raw material with which to realize the potential of contemporary satellite SAR data. The main problem now facing polar oceanographers and sea-ice geophysicists is how to translate the knowledge gained from these SAR experiments into methods of extracting useful information from satellite systems. This section outlines some of the practical difficulties encountered in applying SAR data.

A major difference between satellite and airborne systems is due to their inherent revisit capability and imaging swath width. Aircraft can revisit a surface site many times, offering high spatial and temporal resolution, while a polar-orbiting satellite SAR is at best every 3 days with ERS-1 [25]. Conversely, the satellite has an indefinite revisit (over long timescales of months to years) and greater spatial coverage, but with slightly reduced spatial resolution. Each of these approaches has its drawbacks, and more often than not there is a tradeoff.

A. Temporal and Spatial Resolution

The capability to 'revisit' or repeat an image of an area on the ground has an impact upon the regional monitoring of lead areas or motion-induced divergence in the ice cover. Aliasing of observations of the areal extent of open water and thin ice is a topic, for instance of considerable interest to recovering information about the salt flux and heat exchange between ocean and atmosphere. Is a repeat cycle of three days sufficiently high temporal resolution to monitor the process of new ice formation in leads for instance? It is clear from examples shown in the section 5, that the exact date of lead opening is critical for a number of reasons. Primarily ice growth is

most vigorous during the early growth phase, throughout the period of the largest ocean-atmosphere heat exchange. Concomitant salt fluxes during this phase are significantly higher, and thus dating the opening of a lead is critical to understanding the impact upon the upper ocean, Equally importantly the SAR repeat period is critical to observing seasonal ice zone features, as the timescales of features in the marginal ice zone are susceptible to rapid changes in thermodynamic and dynamic forcing. Consequently, repeat periods of 3 days, typical for ERS - 1 SAR, are unsuitable for some MIZ monitoring and most applications must rely on snap-shot images.

Orbits with longer repeat cycles often have sub-repeat cycles allowing imaging of a similar area on the ground at shorter intervals. Processing orbits such as that of the 35-day repeat orbit phase of MM-1, allowed 3-day repeat imaging and tracking of an moving patch of sea-ice over a longer period, provided that ice motion was westward and consistent with the precession of the orbit and that ice floes and features within the swath arc larger than the resolution limit. Major problems occur in (i) regions where the circulation patterns dictate that the main velocity vector component is in a direction opposite to the orbit precession; and (ii) in marginal ice zones where ice drift velocities exceed around 0.6 m/s. Under these circumstances it is impossible to track the ice over long time periods and distances.

Spatial resolution in SAR data is superior to most alternative data sources and is sufficient for most applications except special cases found in marginal ice zones. Drinkwater and Squire (1987) observe that ice floe tracking becomes almost impossible when floes decrease below the resolving power of the sensor and ice concentrations arc high. In spite of the problematic tracking some information may be drawn from the patterns formed by the modulation of backscatter due to floe size or floe edge distributions (see section 4).

Increasing spatial resolution in order to solve the problems stated above is a thorny issue, because while limiting the study of marginal ice zones and narrow features such as leads, data volumes are already at a level which makes image products unwieldy. Studies have shown that for the majority of cases ice pack monitoring can successful] y utilize low 100 m resolution images. Such is the case that all Alaska SAR Facility image post processing to ice motion velocity fields and ice type grids is currently performed on 100m degraded resolution image data. The only short-term solution to recovering higher resolution data in seasonal ice 7.ones is to usc higher resolution aircraft SAR.

B.   Spatial Coverage

Satellite SAR has a large advantage over aircraft data when it comes to applications of the data requiring monitoring of processes responding to synoptic scale ocean and atmosphere dynamics.

A typical 100 km swath from a satellite data is sufficient to conduct mesoscale or regional studies, and contiguous image strips can be used to trace events over wide areas in the along-track direction. In some cases where it is impossible to monitor ice motion orthogonal to the swath and in the wrong direction (counter to orbit precession). The latter problem may be overcome by a SAR system with the 'flexibility to image much wider areas. Radarsat is capable of imaging a 510 km swath (Table 11), and offers the geographic coverage required to enable complete mapping of the Northern and Southern 1 lemisphere icc covers every 6 days. Only then will it be possible to track parcels of sca icc indefinitely in space and time, or indeed throughout an entire ice season. The capability of RADARSAT to image expansive areas on a weekly basis goes a long way to solving most of the problems associated with applying SAR data to geophysical problems. An additional feature which allows variable viewing geometry using multiple beams will enable beam steering to overcome the difficulties of ice monitoring in problematic regions of icc contraflow or particularly dynamic ice margins.

4.   CM-WAVELENGTHS AND SEA-ICE GEOPHYSICS

"l'o-date a large number of studies have been conducted in order to understand the interaction of microwaves with sca icc [26, 27, 28]. Rather than to describe each of these findings in detail, in this section a number of important findings arc summarized to identify restrictions to using data with known parameters under certain snow and icc conditions or season. For a more detailed review of the physical basis for microwave interactions with sca ice see I lallikainen and Winebrenner [29]. A complete breakdown of results from microwave SAR studies is also provided by Onstott [12].

A.   impact of Frequency

Microwave image content depends on the proportion of the transmitted power reflected or scattered back to the radar. One key to using SAR for studying-sea ice geophysics is the fact that backscattering and the penetration depth through the snow-cover into the ice are frequency dependent. At shorter cm-wavelengths such as X-band, electromagnetic radiation barely penetrates beyond the surface of higher salinity sca icc scattering largely at the ice surface. Onc argument is whether enough information can be gleaned from the characteristics of this scattering for fundamental geophysical differences within the sea ice body to be recognized. The converse strategy is to employ wavelengths longer than 1.-band to penetrate the icc layer and sense the structure and morphology of the icc from the volume scattering which originates from internal inhomogeneities.

Microwave Signatures of Icc Types
Recognition of various components of an icc cover by way of unique frequency-dcpcndcnt backscatter signatures has long been considered the best route towards recovering information on

ice thickness. Since microwave techniques have proved unsuccessful in deriving the thickness of the ice cover, the best direct alternative was considered to be to map ice classes reflecting age or thickness through their salinity or roughness related backscattering 'signature'. Here we briefly describe the success or drawbacks in recovering information using this approach.

Figure 1 shows a heuristic model of the growth of sea ice and provides an indication of the relative importance of various geophysical parameters upon components of C-band SAR backscattering. The model represents the thcrn~odynamically -influenced changes in the relative importance or efficiency of the snow and ice scattering upon the total backscattered signal at a typical satellite SAR incidence angle of about 20°.

First-year Ice

As sea ice grows and ages the corresponding backscatter signature changes. Providing ice grows thermodynamically without deformation it would follow a growth sequence similar to that depicted in Fig. 1. Obviously ice growth can begin in a given location at any time of year, but Fig. 1 simply shows an uninterrupted and complete growth cycle of first-year ice. From its origin as new ice between 10- 20cm thick it is an extremely efficient scatterer, due to its high salinity. If smooth, thin ice appears as the lowest power target in a SAR image, since surface roughness also determines how strong backscatter occurs. Thus the amount of deformation of the thin ice types is critical to the discrimination of thin ice in SAR images [12, 29]. Pancake ice, which undergoes wave disturbance during growth, can in contrast appear extremely rough at all wavelengths from X- to L-band. Thus the icc growth environment is critical to the signature of thin ice types. An anomalous situation observed by various authors for young sea ice is documented in Fig. 1 as a dotted line in the early part of some of the panels. The so-called frost-flower cycle may roughen thin ice to the extent that this high salinity surface causes high backscatter values which can be confused with other ice types [30].

As ice grows through an intermediate stage known as gray ice and into thick first-year (FY) ice, its surface grows colder and rougher, and acquires a snow cover. Moreover, the lower electromagnetic absorption becomes with age the higher backscatter becomes. 'l'bough this argument appears counter-intuitive, various competing effects serve to override the reduced reflectivity caused by reduced salinity and the impedence matching effect of a snow cover. For instance, the snow cover may induce ice surface roughening, whilst also raising the temperature at the snow/ice interface by insulation. 'l'bus, despite thicker FY ice being less saline than new or gray ice, its backscatter is often observed to be roughl y 5d13 higher than younger ice forms in the range 1- 10 GHz [31, 12].

Multiyear Ice

First-year ice thick enough to survive the summer melt becomes multiyear (MY) or old ice (signified as a dashed line in Fig. 1). Typically MY ice is morphologically distinctive with the upper ice consisting of freshened raised areas with a bubbly, low-density upper layer [32]. The process of melt-freeze temperature cycling and the flushing of brine produces low salinity ice which generally supports a deeper winter snow cover. Winter SAR observations of old ice in the Arctic at frequencies of 5 GHz and above indicate that this ice has the strongest backscatter (around -10dB at 23°) of any target other than pancake ice or thin ice with frost flowers. It appears that the lower salinity of this old ice enables greater transmission, lower absorption and deeper penetration into the ice volume. Air inclusions, inhomogeneities and bubbles in the lower density upper ice cause strong volume scattering sufficient to dominate over the corresponding levels of snow and snow/ice surface scattering.

Transmission and Absorption of Microwave,!

Transmission of microwaves in sea ice is determined by scattering and absorption within the medium. These two components arise from the salinity anti age of the sea ice, as well as structural transformations which the ice undergoes. As sea ice ages it becomes desalinated [32] and what begins as relatively high salinity young first-year (FY) ice (> 10ppt salinity) becomes less saline as it thickens, Multiyear ice (MY) more than 1 year old normally has lower salinity after experiencing summer melt processes, and is generally lower than 2-3ppt salinity. Plots of absorption and modeled penetration depths arc shown in Fig. 2 for the typical range of salinity [27, 29]. Firstyear ice (FY) ice typically attenuates a transmitted wave rapidly within a few tens of cm of the surface of the ice, and of the available SAR systems, only L- and P-band can sense deeper than 50cm under most natural conditions. In contrast, cold MY ice experiences frequency-dependent penetration depths varying (in theory) from 1 m at X-band up to several meters at L-band, The result of penetration into MY ice at frequencies higher than C-band is that 'volume' scattering from inhomogeneit ics wit hin the ice becomes dominant [12]. It is this factor which results in old, lower salinity ice having a backscatter value greater than most other ice types. This characteristic allows multiyear ice to be distinguished from lower backscatter FY ice types in C-band aircraft and ERS- 1 data.

The early focus in SAR systems was on longer microwave wavelength systems such as 1.-band and Seasat recovered useful mesoscale information on ice concentration, floe sizes and shapes. The L-band wavelength is too long, however, to sense the microscopic differences between FY and MY. Notwithstanding this drawback, L-band responds most effectively to macroscopic internal deformation and structural features within the ice such as pressure ridges and pressure zones, and leads or fractures. A shift to favour shorter wavelengths was because of the greater responsiveness to ice surface dielectric diffcrcnccs and roughness, While X-band SAR is often touted a being the best ice salinity discriminator, there arc trade-offs in the information content provided by different frequencies and polarizations. The impact of the snowcover is onc serious

limitation to recovering information about the sea ice, due to the reduced penetration of short wavelengths in wet snow. This is treated later in this section.

B.   Polarization Diversity

Until the European Space Agency's planned Envisat polarimetric mission in the 21 st century, the next decade in satellite remote sensing is restricted to single channel instruments. Additional polarization information provided by polarimetric airborne systems at first sight appears inapplicable in the context of conducting current satellite SAR geophysical studies, However, results from recent studies show that the polarimetric airborne SAR is a welcome complement to single-channel SAR.

Scattering model development
Polarimetric SAR provides complex backscatter coefficients at different combinations of linear polarization, These enable the scientist to synthesize or reconstruct a backscatter image for any selected polarization of the incident wave. Recent results using JPL AIRSAR data illustrate the advantage which additional polarizations give in obtaining a more thorough understanding of scattering fundamentals [33]. These data are now being used in developing models and analysis tools required for interpreting the physical basis of single channel sea-ice signatures [34]. Development and testing of fully polarimetric backscattering models is critical because multi-channel techniques are the only way to completely characterize key ice properties involved in the scattering process. Ultimately, backscatter model inversion using SAR image data will require incorporation of all essential scattering physics before realizations of solutions containing the kcy physical properties of sea icc can successfully be made.

Distinguishing between water and ice
The main deficiency of single channel SAR techniques is that the dielectric constant at the surface of smooth new ice can be sufficiently high that thin icc is indistinguishable from ocean water (on the basis of low backscatter magnitude). On the other hand wind waves often generate rough surface scattering for open water in leads which can easily exceed the backscatter of the brightest MY ice target (-8 dB). Both situations cause difficulty by these contrast reversals as they confound automated techniques to study lead openings or ice edges,

L-band polarimetric data and models have recently been coupled to demonstrate (hat it is possible to discriminate unambiguously between open water and young icc (in the range 0-30 cm). This approach requires that the incident wavelength be sufficiently long that it can penetrate and sense the bottom of the high salinity thin-ice layer. For smooth undeformed icc in leads, Winbrenner et al. [35] indicate that small perturbation surface scattering theory is valid. Backscatter is then independent of surface roughness and instead dependent on the dielectric constant. Using an approach suggested by Winebrenner et al. [36], Drinkwater et al. [37]

demonstrate that vv/hh polarization ratios can conveniently be used to resolve differences between water and new ice based on the order of magnitude differences in dielectric constant.

Resolving Ambiguities in Sea-Ice Classification

Rignot and Drinkwater [38] use JPL AIRSAR data to show that multi-channel data can be used to resolve ambiguities or difficulties in discriminating important types of ice at C or L-bands. Fully polarimetric data is more adept at classifying thin ice, while also distinguishing a number of unique FY signatures, and can be used to generate a detailed ice-type chart, The value towards ' satellite SAR data is demonstrated when these fully polarimetric data arc degraded back to their single channel single-polarization constituents. Comparisons of ice classification charts using C-band vv (ERS- 1 simulated) or 1.-band hh polarization data (J-ERS-1 simulated) with the fully polarimetric charts arc used to quantify errors or deficiencies in classification using current single-channel spaceborne SAR. The Rignot and Drinkwater study [38] also shows that combining L-band hh and C-band vv image data from 111{ - 1 and J-ERS-1 would be a more powerful tool for studying sca ice than a single dataset.

c.   Snowcover: A thermal insulator and microwave blanket

Snow plays a critical role geophysically and in terms of microwave backscattering. Dry snow has a higher albedo than sea-ice thereby reflecting a higher proportion of incoming short-wave radiation, but it also tends to increase the physical temperature at the sea-ice surface by virtue of its low thermal conductivity. Snowfall upon sea ice plays a significant role in determining the subsequent heat balance at the surface of the sca ice duc to the insulating capacity of the snow layer. In an analogy to its thermodynamic effect snow also regulates transmission of microwaves. Snow depth, grain morphology, and structure while dependent on the thermal atmospheric forcing also play a significant role in the microwave scattering and absorption of penetrating microwaves.

Dry Snow

The winter snow is laid down with negligible melt metamorphism, and precipitated crystals become broken down and compressed by wind drift. This fine-grained dry snow is effectively transparent to microwaves, and the loss factor shown in Figure 3 is of the order of 15% of the value of pure ice. Having a small dielectric constant (Fig. 3a,b) and low absorption coefficient, it allows microwaves to propagate over long distances up to several meters (Fig. 3c) before being completely absorbed, Typical snow depths on thick FY and MY ice in the Arctic therefore present little impediment to incident microwaves. Additionally, the dielectric constant of dry snow is sufficiently low that the impedence between air and snow is almost matched, This results in negligible surface scattering or internal volume scattering and most of the wave being

transmitted into the snow before being scattered at the snow/ice interface - where the largest dielectric contrast is encountered.

'l'he assumption of a structure-free snowpack is somewhat unrealistic for most naturally occurring snowcovers. After snowfall, thermal gradients through the snowpack promote change snow crystal shapes and sizes, and influence the backscatter. Snow metamorphism and vapour fluxes can result in internal layers causing surface scattering contributions or even Rayleigh volume scattering from enlarged snow grains (at X- and C-bands). Mätzler [39] describes some of these effects upon microwave signatures. The most significant effect occurs when a snow cover develops layers with different density and crystal characteristics. The effects of metamorphism, seasonal melting and refreezing which promote such layering arc described later.

Wet Snow

When snow melting occurs the liquid water which appears in the air-ice mixture dramatically change the influence of snow upon incident microwaves. In contrast to dry conditions, wet snow has a permittivity ε' which becomes frequency dependent (Fig 3a.). Equally it has a dielectric loss c" between 100 and 300 times as large as dry snow and which tends to 1.0 at X-band [40]. As snow wetness increases to 2% by volume, incident microwaves at frequencies above 5 GHz are absorbed at a rate of tens of dB/m. Mätzler [39] measures an absorption coefficient of 0.24/cm in moderately wet snow, and this translates into the penetration depths shown in Fig. 3c.

Frost Flowers

Riming upon sea ice, commonly known as frost-flowering, is a process by which a snow cover may develop upon the surface of the sea ice without mass input from falling snow. Drinkwater and Crocker [30] identified this as a special case in terms of radar scattering because the rime crystals adsorb brine expelled onto the surface of the rapidly growing ice sheet. 'l-his creates an extremely high dielectric constant layer which is an efficient rough-surface scatterer at frequencies higher than C-band [30]. Recent ERS-1 results indicate numerous situations in which frost-flowers appear to bc a tractable an explanation for the high C-band backscatter (- -10 dB), while surface scatterometer experiments by Onstott (personal communication) confirm that their backscatter may reach values more typically associated with the brightest MY ice floes, Their occurrence certainly causes the highest known values of C-band backscatter associated with FY ice, other than pancake ice.

Natural occurrence of such features remains dependent upon a number of special atmospheric and ice growth conditions. Richter Menge and Perovich (personal communication) recently studied natural forms of frost-flowers and made detailed measurements of the brine content of the flowers. Laboratory measurements by S. Martin (personal communication) serve to identify conditions under which they may form so that their appearance in satellite data can be used as a

flag for specific environmental conditions. It is clear however, that their occurrence is closely linked to high heat flux or humid situations where a vapour source combines with an advective term over a relatively cool thin icc surface for the growth of needle or feather-like hoar crystal growth. These features are observed to be highly ephemeral and can appear and disappear overnight depending on wind or snowfall conditions. Their appearance in ERS- 1 data indicate that they may on young sea icc in leads for up to 10 days (K wok, personal communication).

D.   Seasonal Considerations

The main seasonal driver is the fact that the air and ocean temperatures modulate the thermal conditions within the sea ice. Ambient air temperatures and surface humidities control the sensible and latent heat fluxes - and through the energy balance control the icc growth and melt. The most significant indicators of the thermal balance of the sea icc are the snow or ice-surface temperature (in the absence of snow) and the snow/ice interface temperature. These enable the thermal state of the sea ice and surface snow to bc determined. Seasonal changes due to thermodynamic forcing from the atmosphere bring about the most significant changes in the microwave response of the sca ice. Figure 1 depicts some of these changes by way of the introduction of liquid water into the snowpack during spring melting and disappearance of snow during summer. The effect of microwaves encountering wet snow has been described in detail but its consequences for information retrieval have not. Snow wetness and the seasonal impact upon sea ice properties have a considerable impact upon the backscatter contributions from the snow and ice.

Figure 1 indicates that for the most part data on ice growth during fall freeze-up signify a rapid stabilization of backscatter signatures when the temperatures fall below -1 0°C [41]. Up until this point in time early snowfall can impacts scattering by absorbing surface brine on the young ice sheet, thereby increasing snow absorption. Temperature cycling during diurnal cycles also has an impact upon the total backscatter if liquid water appears in the snow. 'l'his is represented in Fig. 1 as ripples during the early Fall period. Generally during the Fall, the ice and snowcover reflects the net heat flux environment, and the rapid stabilization of signatures shown by Drinkwater and Carsey [41] probably reflect the transition to a negative heat balance.

Ice growth continues steadily into the winter, with an accompanying increase in mean snow depth. The winter snowcover in the Arctic and Antarctic has been observed to be an extremely complex medium, with layering occurring as a result of natural radiative processes under atmospheric forcing. This results in layers often of significantly different densities, and salinities, resulting in some internal scattering when the gradients in properties arc strong enough. The horizontal stratification of naturally grown snowcover develops pronounced vertical density variations at a scale height comparable to the microwave wavelength [39]. The superposition of

waves reflected at various interfaces can produce noticeable interference and polarization effects in ground-based scatterometer data. However, for the most part winter snow-structure effects are limited to frequencies higher than C-band while the spatial variations in the snow properties on the scale of the satellite SAR resolution incoherently averages out such effects .

As shown in Section 3A, the appearance of moisture in the snow has a dramatic effect upon the snowcover. In the pendular situation (shown in Fig. 1) where the snowcover begins to melt (i.e. below 3% wetness) the free-water is retained at grain boundaries by capillary suspension. Microwaves can still penetrate through the damp surface layer, but with some attenuation of the backseat ter from the snow/ice interface [42]. Figure 1 reflects the transition to a saturated snow layer together with the corresponding reduction in the icc surface scattering, Once the snowpack becomes isothermal in the late spring, liquid water builds up until the point (>3% wetness) where pore spaces open and liquid begins to drain. This wet snow layer completely masks the sea ice from incident microwaves, preventing sensing of the sea-ice beneath. In this case SAR measurements only provide information on the snowpack on top of the ice layer, or indeed roughness related properties of the ice [43, 44]. It is this rapid change in the snowcover which allows melt detection in ERS- 1 SAR images. Winebrenner et al. [45] exploit the dramatic reduction in backscatter of multiyear sea ice upon the start of the spring melt.

Summer

In early summer the absorption in the remaining surface snow is great. When no further snow is present upon the surface of the sea ice, then the backscattered signal is dominated by the surface roughness and the density and wetness at the surface of the ice floe. During summer conditions the surface roughness dominates the scattering situation and the morphological characteristics of ridges and the structure of ridging zones become more clear. Under these conditions FY and MY ice become indistinguishable.

F.   Validation Measurements and Surface Proof

Surface geophysical data collection has for many years been the accepted form of validation data for remote sensing. It is becoming more and more accepted that remote sensing will lead acquisition of basin-wide information with temporal and spatial coverage far superior to surface experiment data. The term 'ground truth' is thus outdated and requires revising now some SAR techniques are becoming accepted as truth with the accuracy and precision bounds of the measurement technique. It is proposed that for SAR to make the transition to becoming an accepted form of quantification of certain sea-ice geophysical parameters, the term be renamed to some other term such as 'surface-proof'.

To make more powerful scientific usc of SAR products, physical models for sca ice and snow must be successfully married to backscatter models to understand the thermal or dynamic cause or effect of observed signature changes. In accordance, the style of making surface validation measurements must be more rigorously linked to the requirements of these models so that they directly support this association. Continuing development of microwave models is necessary to understand icc signature variability but the kcy to making geophysical measurements with SAR data is to remove these models from the abstract world and realign their development with accepted geophysical models explaining dynamics or thermodynamics of sca ice. Surface experiments must make associated measurements of variables characterizing the forcing behind changes in physical properties (such as the radiation balance) in order that these relationships can be exploited, The following section attempts to build on this theme.

infrequent point measurements in space and time are the main limitation of surface measurements and so the whole approach to providing validatory data must be revisited. In light of the fact that future Radarsat data will provide entire weekly coverage of sea icc in both hemispheres it is difficult to conceive of a scheme for comparing surface proof measurements and geophysical products from SAR data. The answer probably lies in the judicious use and careful positioning of instrumented buoys, and the continuation of well-crafted and coordinated surface measurement programs. Such efforts must endeavour to support those scientists using the latest generation of models by accurate quantification of the most relevant geophysical characteristics of the sea-ice cover. As such these validation experiments will continue to bc a necessary part of scientific utilization of SAR images .

5.   COUPLED DATA ANI) MODEL APPROACIIES

In the previous section, the basis for making sea-ice geophysical measurements using SAR data is discussed. In this section, some examples of potential applications arc considered which couple SAR and surface measurement data. The first example is taken from a microwave modelling exercise using polarimetric SAR data from the J]]]. AI RSAR. The second set of studies uses SAR and various forms of on site data acquired during the Antarctic Winter Weddell Gyre Study in 1992 (WWGS '92). These applications arc chosen as being both somewhat different from the traditional uscs of SAR data, and pertinent to oceanographic applications,

Two kcy development applications for SAR in polar regions arc (i) monitoring of the icc motion and estimation of the freshwater flux, and (ii) calculation of the dynamic thinning caused by ice divergence and model estimates of the corresponding icc growth in ncw leads. The former is now a realizable goal with forthcoming contiguous SAR coverage from Radarsat. When coupled with observations of surface temperature these observations can bc developed to give extra information on surface heat flux and inferences regarding the salt flux from the sea ice.

A, Microwave Scattering Models and Inversion

'I'o-date many theoretical models developed to simulate backscattering from snow and sca icc could not account for many geophysical situations in snow-covered sea icc because they were poorly related to the physics of snow and ice. in many cases this is duc to assumptions inconsistent with naturally occurring ice, or because they try to match abstract internal parameters with realistic or naturally occurring properties. Model development is proceeding at a rate which will soon catch up geophysical applications [35]. Polarimetric models such as that developed by Nghiem [34] arc being tested using polarimetric SAR data in the manner described in section 4. One advantage is that the frequency and polarization sensitivity in the model can be fully tested,

The problem with most scattering models is that they are only valid within a particular range of frequency, ice roughness, or ice salinity. Examples of testing a model's capability under well defined and characterized surfaces are proving most successful [35]. An example of L-band results from tests of a model developed by Nghiem et al. [34] are shown for a thin ice sheet in Fig. 4. Results from matching the model calculated values with conventional backscatter coefficients indicate a good comparison in Fig. 4a. This simulation explains that the backscattering from thin ice requires a high salinity surface expressed as a brine skim or slush layer, in order to explain differences between these vv and hh polarized backscatter data. Behaviour of the complex correlation between hh and vv polarized backscatter is expressed as a magnitude and phase in Fig. 4b and 4c. The magnitude of this correlation clearly expresses a decrease with incident angle, while the phase remains close to zero. This trend is explained by the relative contributions of scattering from the surface and volume over this incidence angle range. While surface scatter dominates up to angles of around 30° incidence, volume scatter becomes dominant beyond this point. Waves penetrating the ice sheet which undergo internal scattering become decorrelated an hence the reduction in |ρ|.

Thus, modelling efforts arc necessary to clarify the physics and electromagnetics governing interactions of microwaves with sea icc at various wavelengths and polarizations [35]. Recent fully polarimetric models must be tested, refined and validated so that they can be used to provide information about icc fabric. By obtaining knowledge of the structure and dielectric properties of sea ice through microwave scattering models wc form a basis for measurement of indicators of ice salinity, thickness and strength, together with the flux environment regulating ice conditions.

B. Wind-Driven Ice Motion and the Momentum Balance

One important geophysical question is how sca icc responds to forcing from above and beneath by winds and currents, as the transfer of momentum to the sca ice is critical to understanding sea

ice dynamics. This argument may be extended to the way ice motion responds to local winds causing discontinuous ice motion or divergence and the formation of leads. A major uncertainty in calculations of regional air-sea-ice heat exchange is the rate of ice divergence.

in this section pairs of Antarctic ERS-1 synthetic aperture radar (SAR) images are coupled with data from Argos buoy data to derive the ice kinematics and divergence in response to the surface wind forcing. The current state of the art in routine post-processing of image data allows tracking of sca ice features. Geophysical data products generated at the Alaska SAR Facility through the Geophysical Processor System (GPS) are; (i) ice motion vector fields, made from pairs of images separated by a fcw days in time from successive passes over the same ice; and (ii) ice classification images [46, 47] and an example illustrating these products from the Beaufort Sea is shown in Fig. 5. The motion field maybe used simply to generate a deformation field in which the gridded relative displacements can be used to measure divergence or convergence in the ice together with the spatial derivatives in both the x and y image directions. This approach is currently being extended at JPL to ERS-1 data products recorded for Antarctic ice. An example of a GPS ice motion product is shown in Fig 6a,b together with the location of the image pair in relation to the nearest Argos buoy.

In the unenclosed Weddell Sea, Antarctica, ice motion is lcss affected by internal stresses generated by coastal contact. In situations away from the coast under largely divergent conditions, onc may assume that the mean ice motion $\overline{\mathbf{v}}_i$ is steady and in balance with the mean current and the mean geostrophic wind $\overline{\mathbf{U}}_g$

$$\overline{\mathbf{v}}_i - \mathbf{A}\overline{\mathbf{U}}_g - \overline{\mathbf{c}}_i = 0.$$ (1)

A simple relationship then exists between the instantaneous time-valying part of the ice velocity $\mathbf{v}'_i$ and the instantaneous geostrophic wind $\mathbf{U}'_g$ [7]

$$\mathbf{v}'_i = \mathbf{A}\mathbf{U}'_g + \mathbf{c}$$ (2)

where the error term e contains all error sources including time-varying current and the divergence in the internal ice stress tensor. importantly, the mean error term $\overline{\mathbf{c}}$ is zero which accounts for its absence in Eq. (1). Matrix $\mathbf{A}$ in each case may be considered a complex scale factor IAI, giving the magnitude of the ratio of ice speed to wind speed, and a rotation or turning angle b (positive - clockwise) between the ice and the wind vectors. Similar schemes have recently been used by Martinson and Wamscr [48] and Kottmeier and Engelbart [49] to explain the drift of sea ice in the Weddell Sea.

Wamser and Martinson [50] demonstrate that a free-drift form of the ice momentum balance can be successfully used under divergent conditions to simulate observed Eastern Weddell Sca ice

drift, with some assumptions regarding ice-water drag and internal ice stress. 'l'o-date this approach has been used for two buoy drift experiments to derive the typical range of winter Antarctic 10 m drag coefficients [48, 50]. in 80-100% concentration ice they observed air-ice values in the range $1.45 \times 10^{-3} \leq C_{10} \leq 1.79 \times 10^{-3}$ with aerodynamic roughnesses spanning $0.27 \leq z_0 \leq 0.47$ mm, and derived a value for the icc-ocean drag coefficient of 1.13×10^{-3}.

Data shown here characterizes ice motion in the Eastern-Central Weddell Gyre, in an area of Argos drifters deployed by the Germans from the research vessel Polarstern in July 1992 during the Winter Weddell Gyrc Study **(WWGS '92).** Figure **6** indicates selected results from these SAR images and buoys placed in the Central Weddcll Gym. in Fig. 6a the position of two geolocated ERS-1 SAR images arc shown with respect to the July portion of the drift track of buoy 9364. In Fig. 6b the corresponding SAR-tracked ice motion is shown for a 1 day period between this pair of images acquired on 13 and 14 July. In Fig. 6C the drift velocity of Buoy 9364 responds quickly to pulses in the geostrophic wind U_g' (calculated from the two-dimensional buoy pressure gradient field) and drifts along the track depicted in Fig. 6a. The corresponding response to U_g' of the area encompassed by a triplet of Argos buoys including 9364 is equally sensitive, The area encompassed by this buoy triplet increases consistently over the month of July in response to the wind stress (Fig. 6d) and the area of new ice production in this period is 1100km2, equating to a mean divergence of $0.67 \pm 0.45\%$/day. Sea ice quick] y reacts to pulses in geostrophic wind, as is reflected in the 24-hr smoothed divergence in Fig. 6d. Each pulse of relatively stronger winds is interleaved by relaxation events where the ice pack converges and leads close under internal stresses. in contrast, divergence over the whole six-buoy array in July results in a mean value of $0.4 \pm 0.6\%$/day. South-eastern buoys tend to converge over the same July period and such spatial variability in the divergence results in a lower mean and larger variance than that represented in Fig. 6d. This spatial variability in divergence, on different scales makes it imperative that the satellite data are additionally employed in monitoring regional divergence and **hence new ice** production.

The ice motion derived from the SAR motion field in Fig. 6b indicate a mean ice motion vector magnitude V_i of 0.255 m/s, with a bearing θ_i of 17.466° (when the ice motion direction is corrected by -45° to account for the Northern Hemisphere SSM/I grid coordinates used in the motion vector mapping), The mean geostrophic wind U_g over the same period of ice motion shown in Fig. 6b is calculated at 6.3 m/s, on a bearing of 36.5°. Preliminary results comparing these buoy-derived winds with the first Antarctic ER - 1 SAR-derived ice motion give values for $(|A|, \beta)$ of (0.04 , 190). The turning angle is consistent with a mean of IA I = 0.03 and $\beta = 18° \pm 18°$(right of the wind) observed during periods of free drift during WWGS '86 and '89 [50].

Further processing of SAR icc motion data acquired during studies will form a satellite icc-motion database for comparison with buoy statistics of velocity and divergence. The tested

20

relationships between wind-stress and divergence, under essentially free-drift conditions, can also then be extended to yield similar bulk drag coefficients through this simple formulation of the momentum balance. In addition more accurate long-term estimates of divergence can be made in order to make estimates of the impact upon heat exchange between the upper ocean and atmosphere.

c.   SAR and Ice-ocean Model Surface Flux Estimates

    Coupling SAR observations and physical ice growth models

A simple extension can be made of the results shown in Fig. 6 by coupling the regional SAR-derived divergence measurements with an ice growth model. in Fig. 7a the full energy balance is computed using longwave radiation budget and short-wave fluxes (from WWGS '92 shipborne measurements) and estimates of the turbulent fluxes of sensible and latent heat driven by the wind values plotted in Fig. 6. 'I'he energy balance is used in an icc growth model developed by Cox and Weeks [51] to simulate growth of an icc sheet (Fig. 7b) for the month described by the buoy drift and SAR motion data. Typical snow data arc added in the model to reproduce natural observed conditions and with uninterrupted growth the icc sheet reaches a thickness of 55 cm in only 20 days. Figure 7b indicates the salinity and temperature profiles of this icc sheet at 10cm intervals. The corresponding brine volume profiles arc computed as a direct input to backscattering models which require vertical profiles of dielectric properties within the icc sheet. 'I'he direct relevance of this technique for oceanography, however, is shown in Figure 7c and 7d, where the impact upon the upper ocean is monitored by calculating the flux of salt from ice to upper ocean as brine rejection and drainage take place. During early growth, when the air temperatures were close to $-30°C$, winds of between 4 and 10 m/s combined to cause net outgoing sensible heat fluxes of -350 W/m^2. With clear skies and relatively brisk winds the sensible heat flux drive a net heat flux which on Day 205 reaches -500 W/m^2. Resulting ice growth is rapid and the first day the growth rate peaks of, 15cm/d. After this early peak the rate slows to typical values of 2 cm/day. A similar trend is seen in the salt flux data, where at peak growth the salt flux exceeds 65 kg/m^2/month.

This brief example continues from the theme developed using the buoy and icc motion data. Future SAR measurements of regional icc divergence and the fraction of open water, together with the ice growth model presented here will enable regional heat and salt budget to be assessed.

    Time-series Backscatter Data and the Energy Budget

A further extension to our understanding of microwave backseat tering response from sea ice can also be drawn from studying radar backscatter time-series in conjunction with this ice modelling and radiation balance approach. in the final example a time-series of surface C-band

scatterometer measurements is shown during a 3 day Weddell Sea ice drift station at the end of the month of July when the net heat flux budget shows a dramatic transition [52]. Field experiment data from W WGS'92 for a 1 m thick ice sheet in Fig. 8 shows 10 minute averages of wind stress and turbulent sensible heat flux together with the net energy budget (courtesy of W. Frieden of Hannover University, Germany) during a scatterometer time-series data lasting from day 203 to day 206 (21 to 24 July, 1992). In the lowermost panel of Fig. 8 the 45° incidence C-band signature is plotted starting at Julian Day 2.03.79. The solid line with error bars represents the mean vv-polarized backscatter and the dotted line the corresponding hv polarized backscatter. A 10 dB variation in vv polarized and 5 dB variation in hv polarized backscatter is observed in response to the changes in the heat fluxes presented.

Fig. 8a indicates a large variation in wind stress during the period shown, increasing rapidly to over 5 $N/m2$ when the winds peaked at 20 rids. The increase in wind took place with a sudden rise in air temperature (Fig, 8b) from around -23°C to 0°C during the passage of a warm frontal system. As a consequence of the overcast skies, warm temperatures and the high wind, the sonic-anemometer-thermometer recorded a net downward flux of sensible heat (or negative in the coordinate system used by the instrument) which peaked during the strong winds at 60 W/m². A sharp decrease in the amount of incoming turbulent sensible heat occurs on the early morning of 24 July, due to the clear night sky.

A preliminary estimate of the net energy budget is shown in Fig. 8c using the conventional system with "-" illustrating net outgoing heat fluxes of heat and vice-versa for "+". At the start of the period, the surface lost nearly 50 W/m². This energy was supplied by freezing processes as indicated by thermistors placed within the sea "ice and icc core measurements. immediately the sky became overcast the temperatures rise and light snowfall began. Several dB variability in backscatter indicate several orders of magnitude change in scattering over the conditions indicated. The change in heat flux regime is strongly correlated with a reduction in vv and hv backscatter. High winds and a brief period of cloud-free night at Julian Day 206.2 encourage evaporative cooling and a local maximum in the values of vv and hv-pol backscatter. Surface measurements in association with the C-band radar data indicated that the vv-polarized data clearly signal the change in heat flux environment when air temperatures rise above -20°C. When surface temperatures rose dramatically snow-grain transformations began and melting was focused at the surface. Snow had not reached an isothermal state and reductions in backscatter appear caused by an increase in moisture and formation of a surface crust layer. At this time on day 205, the minimum backscatter occurs (Fig. 8d), but the wind speed continued to rise to gale force. During this period a confusing reversal occurs in the vv-pol data with a rise in backscatter values to a level higher than that on day 203. It is confirmed during this period that no significant amount of surface wetness accumulated in the shallow 3 cm deep snow layer. Instead, as Andreas

and Ackley (1982) have pointed out, the wind speeds at the surface can be large enough that enough heat is removed by surface sublimation to prevent visible melting and free-water in the snow. It is suggested that in the case of these strong winds enough heat is removed by sublimation to preclude significant melting, despite a large net radiation balance. The large vapour flux induced in the snow rapidly changed the snow crystal characteristics under these conditions from hoar-style angular crystals (induced strong negative heat gradients up to day **204) to** large rounded crystals. Together with the layering which developed in the snow, it is proposed that these snow changes play a large role by increasing volume scatter. A last significant change in vv-pol backscatter takes place after cooling and overnight refreezing (day 205) of all moisture in the snow layer. Diurnal warming and another swing in the humidity which took place on day 206 resulted in another minima in the backscatter. This shor[-term minimum coincides with the brief period of incoming shor~-wave energy during scattered clouds and probably signifies a brief reappearance of moisture at the surface of the snow.

This winter example clearly indicates that the sea-ice surface properties respond to the balance of fluxes at the surface. Furthermore, a C-band radar reacts equally sensitively to these changes. 'l'bough these temperature swings may be more commonly associated with spring conditions, this change in events may be recognized in time-series data to reflect transformations in the surface heat and vapour flux environment. It is proposed that with the aid of buoy data and weather analysis fields for specifying boundary conditions, the satellite SAR and surface data be used together with physical models to understand how microwave data reflect key changes in the energy balance, The power of time-series measurements using SAR backseat tcr has bare] y been exploited. Coupling an analysis of data in this manner together with the tracking capability of SAR provides a powerful method for studying change.

6.   DISCUSSION AND CONCLUSIONS

The time has come to use SAR remote sensing as a competent sea-ice measurement tool. This requires that we expend time validating approaches and confirming the geophysical utility of the extracted data. Ground-''proof" is the key to establishing SAR as a credible alternative to intensive surface-based experimental studies.

The main problem confronting scientists wishing to exploit SAR remote sensing of the polar ice pack is coping with the vast amounts of data which are being recovered, Automated algorithms which are tested and validated must become the accepted norm, and are a necessary step to digesting the spatial and temporal dimensions of the resulting datasets. The key to realising geophysical applications of these data is realising the requirement to process vast amounts of data routinely, with knowledge of the errors inherent in the post-processing techniques used.

These quantitative data will be used then to reflect not only the changing dynamics Of the sea-ice pack itself, but also to reflect the changing surface heat and salt flux environment.

The application of rapidly evolving algorithms to problems of monitoring sea-ice geophysics is a necessary step to establishing the credibility of microwave SAR. We must all use and validate products of these applications such that the remote sensing SAR tool will become accepted in sca ice geophysics. To make best use of this rapidly evolving tool, however, onc must recognize the drawbacks involved in using aircraft or satellite SAR data. The researcher must appreciate the difficulties of using these techniques so that they can interpret the observations confidently. The objective of this section is to describe the problems and difficulties associated with use of microwave SAR instruments both from airborne and spaceborne platforms, and to outline approaches to minimise the impact of these problems in the geophysical interpretation of the data,

There will be a time soon when the SAR will guide us to geophysical variability which was otherwise unrecognised. Already SAR is demonstrating the utility of the time dimension, often absent in sampling of polar geophysical media duc to the logistical difficulty of routine observations. The goal of future satellite datascts therefore shall be to provide both a Lagrangian time-series of the characteristics and dynamics of sca ice floes tracked across the Arctic basin or Southern Ocean, Parcels of sea ice can be followed through their evolution from thin new ice to multiyear ice using a Lagrangian style sea-ice tracker, This requires observations be frequent, continuous and indefinite over a large geographic expanse, We are already close to this goal when Radarsat arrives with the mandate to map the complete sea-ice cover of both hemispheres once every week. The thought of tracking a piece of icc throughout its lifetime negates the necessity to identify ice "types" - or indeed to usc such types as a proxy for sea-ice thickness. As this chapter has shown, wc are close to marrying physical ice models with microwave scattering models. Providing enough supplementary surface information is available in the form of surface temperatures or wind speeds the full lifecycle of the sea-ice sheet can bc monitored in the context of its surface momentum, heat, salt, and freshwater balance. Within this framework, SAR is already used equally well to monitor variations at a point in space, in a Eulerian framework, In summary, SAR will go a long way to elucidate sea-ice processes influencing the capacity of the high-latitude oceans to regulate global climate.

7. ACKNOWLEDGEMENTS

PIPOR Office, and ESA arc gratefully thanked for their support in Antarctic ERS- 1 SAR 'acquisition scheduling.

8.   BIBLIOGRAPHY

[1]   Fea, M., The ERS-1 Ground Segment, *ESA Bulletin, 65,49-59, 1991.*

[2]   Jezek, K., and Carsey, F.D. (cd.). McMurdo SAR Facility, *BPRC Technical Report, No. 91-01*, Byrd Polar Research Center, Ohio State University, Columbus, Ohio 43210-1308, 31pp, 1991.

[3]   Ebert, E. E., and J.A. Curry, An intermediate one-dimensional thermodynamic sea ice model for investigating ice-atmosphere interactions, *J. Geophys. Res.*, **98**, C6, **10085-10109,** 1993.

[4]   Gordon, A.L., Two Stable Modes of Southern Ocean Winter Stratification, In P.C. Chu and G.C. Gascard (eds.), *Deep Convection and Deep Water Formation in the Oceans,* Elsevier, 17-35, 1991.

[s]   Gordon, A.L. and Huber, B.A., Southern Ocean winter mixed layer, *J. Geophys. Res.*, 95, 11655-11672,   1990,

[6]   Carsey, F.D., R.G. Barry, and W.F. Weeks, Introduction, Microwave Remote Sensing of Sea Ice, *Geophysical Monograph, 68,* Chapt. 1, 1-7, 1992.

[7]   Holt, B. M., D.A. Rothrock, and R. Kwok, Determination of Sca Ice Motion from Satellite images, Microwave Remote Sensing of Sea Ice, *Geophysical Monograph,* **68,** Chapt. 18, 343-354, 1992,

[8]   Martin, S., B. Holt, D.J. Cavalieri, and V, Squire, Shuttle imaging radar B (SIR-B) Weddell Sea ice observations: a comparison of SIR-B and scanning multichannel microwave radiometer sea ice concentrations, *J. Geophys. Res.*, 92, C7, 7173-7179, 1987.

[9]   Massom, R., *Satellite Remote Sensing of Polar Regions, CRC* Press Inc., Boca Raton, FL 33431, 307pp., 1991.

[10] Livingstone, C.E, A.L. Gray, R.K. Hawkins, R.B. Olsen, J.G. Halbertsma, and R.A. Deane, CCRS C-band Radar: System Description and Test Results, Proceedings of 11th Canadian Symposium on Remote Sensing, University of Waterloo, Waterloo, Ontario, June 22-25, pp. 503-518, 1987.

[11] Livingstone, C.E, A.L. Gray, R.K. Hawkins, R.B. Olsen, CCRS C/X- Airborne Synthetic Aperture Radar: an R and 1> Too] for the ERS-1 Time Frame, *IEEE National Radar, 1988.*

[12] Onstott, R., SAR and Scatterometer Signatures of Sca Ice, In *Microwave Remote Sensing of Sea Ice,* (cd, F. Carsey), Geophysical Monograph, 68, American Geophysical Union, 73-104, 1992.

[13] Fu, L., and Holt, B., Seasat Views Oceans and Sea ice with S ynthetic Aperture Radar, *JPL Publication,81* -120, 200pp., 1982.

[14] Johannessen, O. M., W.J. Campbell, R, Shuchman, S. Sandven, P. Gloersen, J. A. Johannessen, E.G. Josberger, and P.M. Haugan, Microwave Study Programs of Air-Ice-Ocean Interactive Processes in the Seasonal Ice Zone of the Greenland and Barent Seas, In *Microwave Remote Sensing of Sea Ice,* (cd, F. Carsey), Geophysical Monograph, 68, Chapt. 13, American Geophysical Union, 261-289, 1992,

[15] Roach, A., K. Aagaard, and F.D. Carsey, Coupled Ice-Ocean Variability in the Greenland Sea, *Atmosphere-Ocean*, 31,3,319-337, 1993.

[16] McNutt, L., S. Argus, F. Carsey, B. Holt, J. Crawford, C. Tang, A.C. Gray, and C. Livingstone, The Labrador Ice Margin Experiment, March 1987 - A Pilot Experiment in Anticipation of Radarsat and ERS-1 Data, *EOS Trans.*, AGU, June, 634-643, 1987.

[17] Carsey, F.D., S.A. Digby-Argus, M.J. Collins, B. Holt, C. Ii. Livingstone, and C. I. Tang, Overview of LIMEX '87 Ice Observations, *IEEE Trans. Geosci. and Remote Sens.*, 27,5,468-481, 1989.

[18] Drinkwater, M. R., and S.A. Digby-Argus, LIMEX '87; international Experiment in the Labrador Sea Marginal Ice Zone, *Polar Record, 25,* 155,335-342, 1989.

[19] Raney, R, K., S. Argus, L. McNutt, Executive Summary: LIMEX '89, *RADARSAT Program Office Publication,* 30 Aug 89, 13pp., 1989.

[20] Carsey, F.D, and R. K. Rancy, 1989. (cd's,) LIMEX Special Issue, *Trans. Geosci. and Remote Sens.*, 27,5, 1989.

[21] Asknc, J. (Ed.) The Bothnian Experiment in Preparation for ERS-1, 1988 (BEPERS-88), *Special Issue Int. J. of Remote Sens.*, 13, 13,2373-2489, 1992.

[22] Barber, D., D.D. Johnson, and E.F. LeDrew, Measuring Climatic State Variables from SAR images of Sea Ice: The SIMS SAR Validation Site in Lancaster Sound, *Arctic, 44,* 1, 108-121, 1991.

[23] Barber, D., Assessment of the interaction of Solar Radiation (0.3 to 3.0 μm) with a Seasonally Dynamic Snow Covered Sca Ice Volume, from Microwave (2.0 to 5.0 cm) Scattering, Earth Observations Laboratory Report, *ISTS-EOL-TR93-002*, Univ. Waterloo, Waterloo, Ontario, Canada, N2L 3G1, 266pp., 1993.

[24] ESA, Proc. ERS-1 Results Symposium, *ESA Special Report*, SP-359, 275-375, 1992,.

[25] ESA, ERS-1 System, *ESA Special Publication,* SP-1 146, 87pp., 1992.

[2 6] Ulaby, F.T., R.K. Moore, and A.K. Fung, *Microwave Remote Sensing: Active and Passive,* Vol. 2, Adison Wesley, 1064pp., 1982.

[27] Ulaby, F.T., R.K. Moore, and A.K. Fung, (Eds.), *Microwave Remote Sensing :Active and Passive,* Vol. 3, Adison Wesley, 2162pp., 1982.

[2 8] Carsey, F.D., Microwave Remote Sensing of Sea Ice, *Geophysical Monograph, 68,* American Geophysical Union, 462pp., 1992.

[29] Hallikainen, M., and D.P. Winebrenner, The Physical Basis for Sea Ice Remote Sensing, Microwave Remote Sensing of Sca Ice, *Geophysical Monograph, 68,* Chapt. 3,29-46, 1992.

[30] Drinkwater, M, R., and Crocker, G.B., Modelling changes in the dielectric and scattering properties of young snow-covered sea icc at GHz frequencies. *Journal of Glaciology, 34, 118,* 274-282, 1988.

[31] Livingston, C. R., K.P. Singh, and A.L. Gray, Seasonal and Regional Variations of Active/Passive Microwave Signatures of Sca Ice, *IEEE Trans. Geosci. and Remote Sens.*, GE-25, **2, 159-173, 1987.**

[32] Tucker, W.B., D.K. Pcrovich, A.J. Gow, W.F. Weeks, and M.R. Drinkwater, Physical Properties of Sea Ice Relevant to Remote Sensing, In Microwave *Remote Sensing* of *Sea Ice*, (Ed.) F.D. Carsey, American Geophysical Union, Geophysical Monograph 28, Chapter 2,9-28, 1992.

[33] Drinkwater, M. R., R. Kwok, E. Rignot, }1. Israelsson, R.O. Onstott, and D.P. Winebrenner, Potential Applications of Polarimetry to the Classification of Sca Ice, In *Microwave Remote Sensing of Sea Ice*, (Ed.) F.D. Carsey, American Geophysical Union, Geophysical Monograph 28, Chapter 24,419-430, 1992.

[34] Nghiem, S. V., R. Kwok, S.H. Yueh, and M.R. Drinkwater, Experimental Observations and Theoretical Models for Polarimetric Remote Sensing of Sca Ice, In preparation, 1993.

[35] Winebrenner, D. P., J. Bredow, M.R. Drinkwater, A.K. Fung, S.P. Gogineni, A.J. Gow, T.C. Grenfell, H.C. Han, J.K. Lee, J.A. Kong, S. Mudaliar, S. Nghiem, R.G. Onstott, D. Perovich, L, Tsang, and R.D. West, Microwave Sca Ice Signature Modelling, In *Microwave Remote Sensing of Sea Ice*, (Ed.) F.D. Carsey, American Geophysical Union, Geophysical Monograph 28, Chapter 8, 137-175, 1992.

[36] Winebrenncr, D.P., L. Tsang, B. Wen, and R. West, Sea Ice Characterization Measurements Nccdcd for Testing of Microwave Remote Sensing Models, J. Oceanic Eng., 14, 2, 149-158, 1989.

[37] Drinkwater, M, R., R. Kwok, D. P. Winebrenner, and E. Rignot. Multi-frequency polarimetric SAR observations of sca ice, *J. Geophys. Res.*, **96**, Cl 1,20679-20698, 1991.

[38] Rignot E., and Drinkwater, M. R., Winter Sea Ice Mapping From Multi-Parameter Synthetic Aperture Radar, In Press, *J. Glaciology*, March 1993.

[39] Mätzler, C., Applications of the interaction of Microwaves with the Natural Snow Cover. In *Remote Sensing Reviews,* Vol. 2, pp. 259-387, Harwood Academic Publishers, 1987.

[40] Dierking, W., *Sensitivity Studies of Selected Theoretical Scattering Models with Applications to Radar Remote Sensing of Sca Ice,* Report 33, Alfred Wegener Institute for Polar and Marine Science, Bremerhaven, Germany, 113pp. Nov. 1992.

[41] Drinkwater, M. R., and F.D. Carsey, Observations of the late-surnmer to fall transition with the 14.6 GI Iz SEASAT scatterometer, *Proc. IGARSS '91 Symposium,* Vol. 3, IEEE Catalog #CI 12971-0, June 3-6, 1991, Espoo, Finland, 1597-1600, 1991,

[42] Drinkwater, M. R., LIMEX '87 Ice surface characteristics; implications for C-band SAR backscatter signatures. *IEEE Transactions on Geoscience and Remote Sensing ,27,5,501-513, 1989.*

[43] Livingstone, C. E., and M. R, Drinkwater, Springtime C-band SAR backscatter signatures of Labrador Sea marginal ice: measurements vs modelling predictions. in *IEEE Trans. Geosci. and Remote Sensing, 29, 1, 29-41,* 1991a.

[44] Livingstone, C. E., and M. R. Drinkwater, Correction to Springtime C-band SAR backscatter signatures of l.abrader Sea marginal ice: measurements vs modelling predictions, *IEEE Trans. Geosci. and Remote Sensing, 29,3,472,* 1991b.

[45] Winebrenner, D. P., E.D. Nelson and R. Colony, Observation of Melt Onset on Multiycar Arctic Sea Ice using the ERS-1 SAR, Submitted to *J. Geophys. Res.*, July, 1993.

[46] Kwok, R., J.C. Curlander, R. McConnell, and S.S. Pang, An Ice-Motion Tracking System at the Alaska SAR Facility, *IEEE Trans. oceanic Eng., 15, 44-54,* 1990.

[47] Kwok, R. E. Rignot, and B. Holt, identification of Sea-Ice Types in Spaceborne Synthetic Aperture Radar Data, *J. Geophys. Res., 97, C2, 2391-2402, 1992.*

[48] Martinson, D. G., and C. Wamser, Ice drift and momentum exchange in winter Antarctic pack ice, *J. Geophys. Res., 95, 1741-1755, 1990.*

[49] Kottmeier, C, and D. Engelbart, Generation and atmospheric heat exchange of coastal poynyas in the Weddell Sea, *Boundary Layer Meteorology, 60,207-234, 1992.*

[50] Wamser, C., and Martinson, D. G., Drag coefficients for winter Antarctic pack ice, *Journal of Geophysical Research, in* press, 1993,

[51] Cox, G.F.N, and Weeks, W. F., profile Properties of Undeformed First-Year Sea ice, CRREL Rep., 88-13, 57pp.,1988.

[52] Drinkwater, M. R., Hosseinmostafa, R., and W. Dierking, Winter Microwave Radar Scatterometer Sca Ice Observations in the Weddell Sea, Antarctica, *Proc. IGARSS '9.?,* Tokyo, Japan, Aug. 18-21, 1993.

[5 3] Andreas, E.L., and S.F. Ackley, On the differences in Ablation Seasons of Arctic and Antarctic Sea Ice, *J. Atmospheric Sci., 39,440-447, 1982.*

Tables

Table 1.   Sea ice variables of primary interest for atmosphere-ocean-ice interaction studies.

Parameter	Horizontal Spatial Seal.&.........	Temporal Scale	Accuracy
Ice Extent	100m -1 km	1d - 10y	< 0.1% of ar
Ice Thickness	0 - 100 km	1 d - 7d	10-50 cm
Thin Ice Coverage	1m -10 km	1 h - 10 d	< 1% of area
Ice Divergence	1 -100,000 km^2	1 - 7 d	< 1 Ye/d
Ice Type	10-1000 km	7 d - 1 m	*(1 00/#type
Snow Depth	0-1 km	1 - 7 d	5 cm
Summer Melt	100 - 1 x 10^6 km^2	7 d - 6 m	5% of area
Meltpond Coverage (i.e. Albedo)	0-10 km^2	7 d - 6 m	< 3 % Of are
Ice Motion	0.1-10 km	1 - 7 d	2 cm/s
Icc Growth Rate	0.1-10 km	1 h - 7 d	10 cm /d

Table II.   Specifications of satellite synthetic aperture radars

Satellite	Seasat	ERS-1	J-ERS1	Radarsat
Period of operation	July - Oct. 1978	July '91- present day	Feb. '92- present-da y	to be launched in 1995.
SAR operating frequency	1.275 GHz	5.3 GHz	1.275 GHz	5.3 GHz
Wavelength	23.5 cm	5.7 cm	23,5 cm	5.6 cm
Polarisation	HH	VV	HH	1111
Incidence Angle:	23.0°	23.5°	35°	20-59°
Pixel size		12.5 m		
Resolution: Azimuth	25 m (4 looks)	30 m (4 looks)	30 m (4 looks)	8 - 100 m (1 -8 looks)
Range	25 m	25 m	18 m	8 - 100 m
Swath width	100 km	100 km	75 km	45-510 km
Orbit Repeat Frequency	near-3 d	3 - 35 - 3 d	44 d	24 d
Onboard Storage	No	No	Yes	Yes

Figure Captions

Figure 1.	Heuristic model of the relationships between sea ice physical properties and the nature of C-band microwave interactions, throughout the thermodynamic growth cycle. The lower panel shows potential geophysical information contained in microwave back scatter record.

Figure 2.	Summary of (a) experimental power absorption and (b) equivalent penetration depth in sea ice, after [29].

Figure 3.	Wet snow (a) Permittivity (ε') and (b) loss factor (c") at volume fractions of water of 1 % and 10%, at a constant snow density of 250 $kg\,m^{-3}$, from empirical equations given in [40]; (c) signifies the frequency-dependent penetration depth based on these dielectric properties for varying snow water content from the curves of [40] in (a) and (b),

Figure 4,	Fully polarimetric microwave scattering model results from L-band simulations of thin icc in March 1988 in the Beaufort Sea (after [34]). (a) shows the comparison between vv, hh and hv polarized backscatter data and simulated returns; (b) indicates the magnitude $|\rho|$ of the complex correlation bet ween vv and hh linearly polarized returns; (c) shows the corresponding phase of the complex correlation p.

Figure 5.	Example of geophysical products routinely generated at the Alaska SAR Facility from ERS - 1 SAR data (courtesy Ron Kwok and Ben Holt, JPL). images were acquired in the Beaufort Sca and are separated by 3 days in November 1991. The icc motion vector and resulting deformation grids are shown in the centre panels and the classified images arc shown in the lowermost panels.

Figure 6.	Illustration of ice drift and deformation extracted from Antarctic IRS-1 SAR images and an Argos drifter instrumented site in the central Weddell Sea, Antarctica. (a) Geolocated SAR image locations superimposed upon the July drift track of buoy 9364; (b) SAR image on 14 July, 1992 (Day 196) with superimposed vectors illustrating the icc motion field over a 24 hour period from day 195- 196 [SAR image © ES A]; (c) Ice drift velocity compared with the geostrophic wind in July; (d) buoy triplet area change and computed ice divergence.

Figure 7.	Radiation balance and icc growth during July 1992, in the area of the buoy drift shown in Fig. 6. (a) Radiation balance; (b) ice properties during one month of icc growth starting on day 192; (c) salt flux, net conducted heat flux and icc growth rate during this period.

Figure 8.	Shipborne C-band microwave radar scatterometer time-series comparison with surface fluxes of heat and momentum. (a) turbulent flux of momentum; (b) turbulent flux of sensible heat; (c) the energy balance (d) vv and hv backscatter response with temperature and humidity. Data were acquired during the Winter Weddell Gyre Study in the austral winter of 1992.
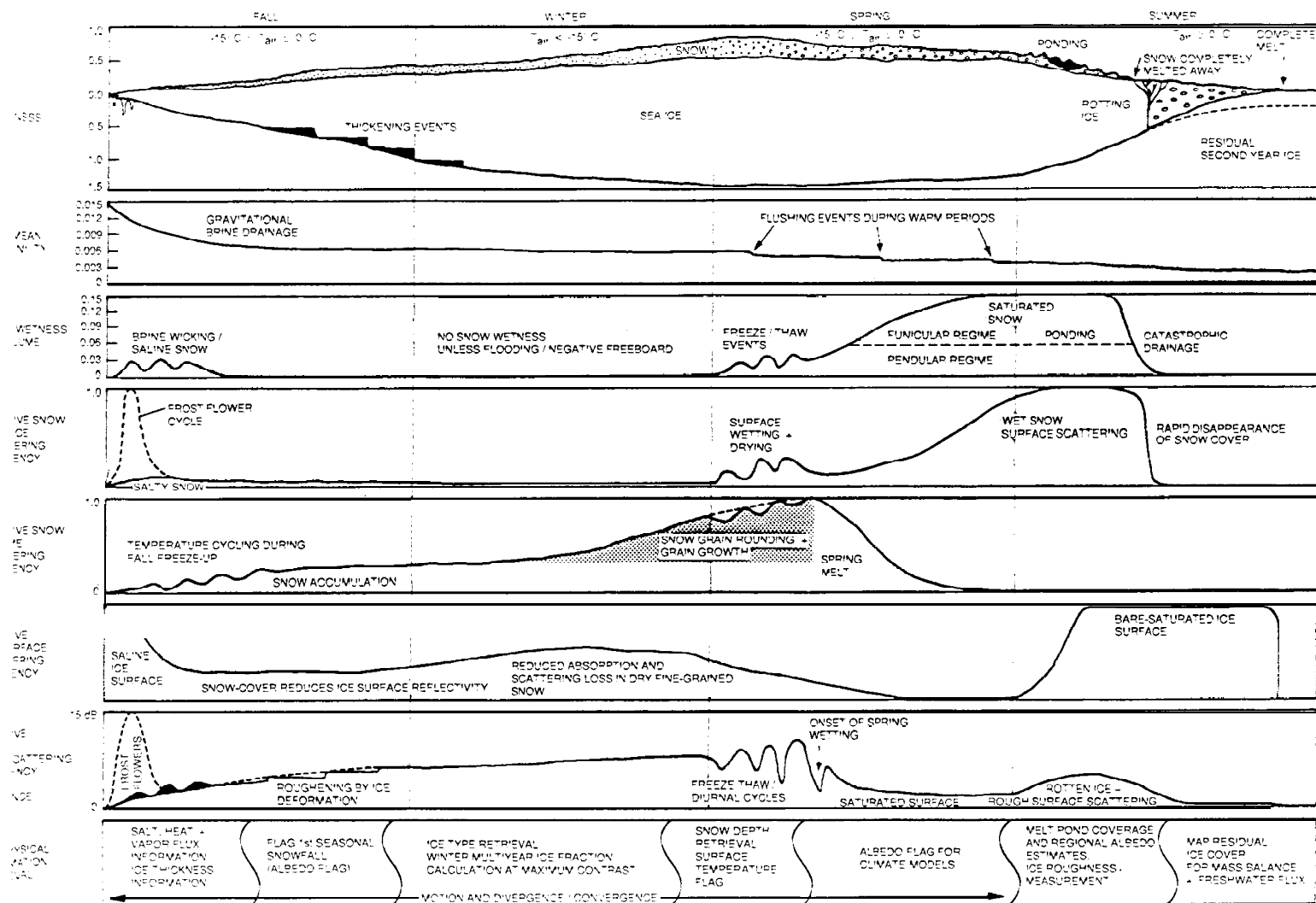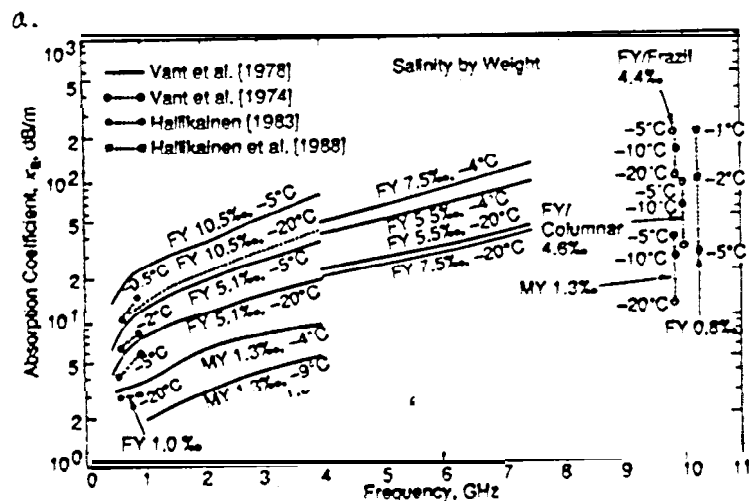
FIG 1

a.

Fig. 3(a) Experiment.d power absorption coefficient of sea ice, obtained by various f nvestigators.
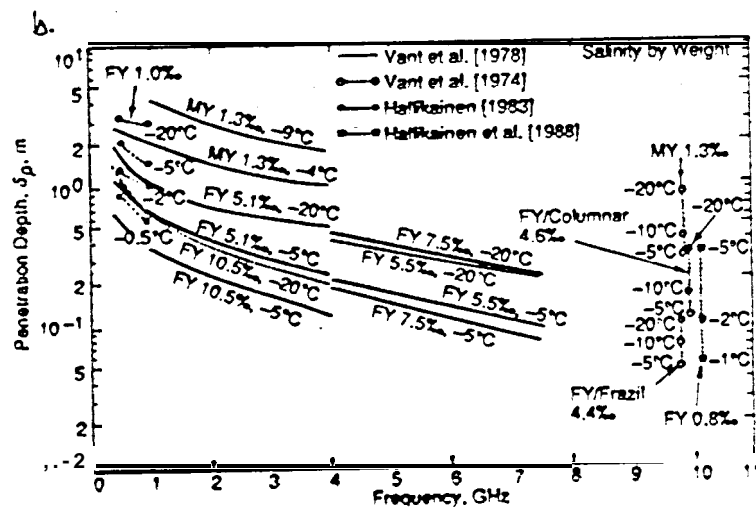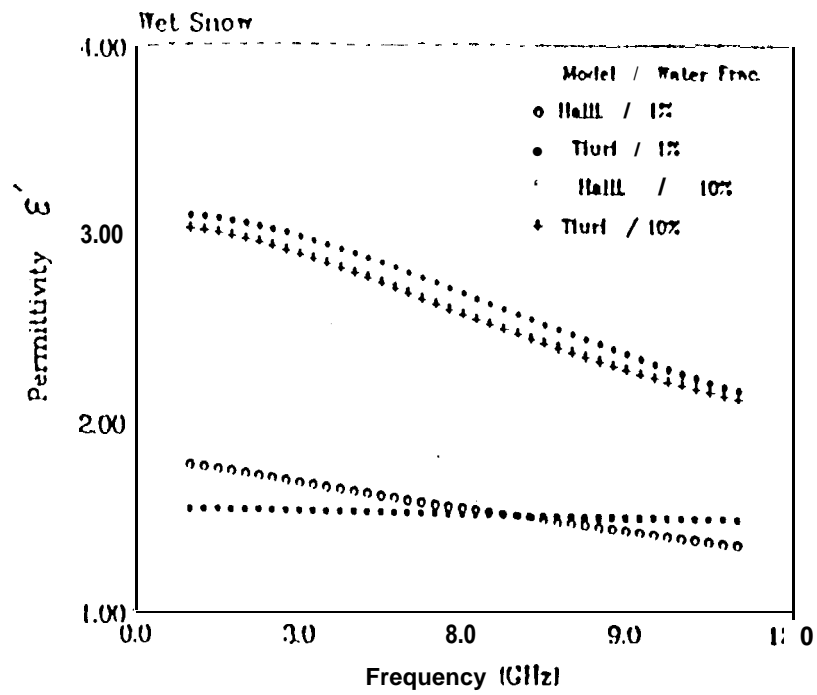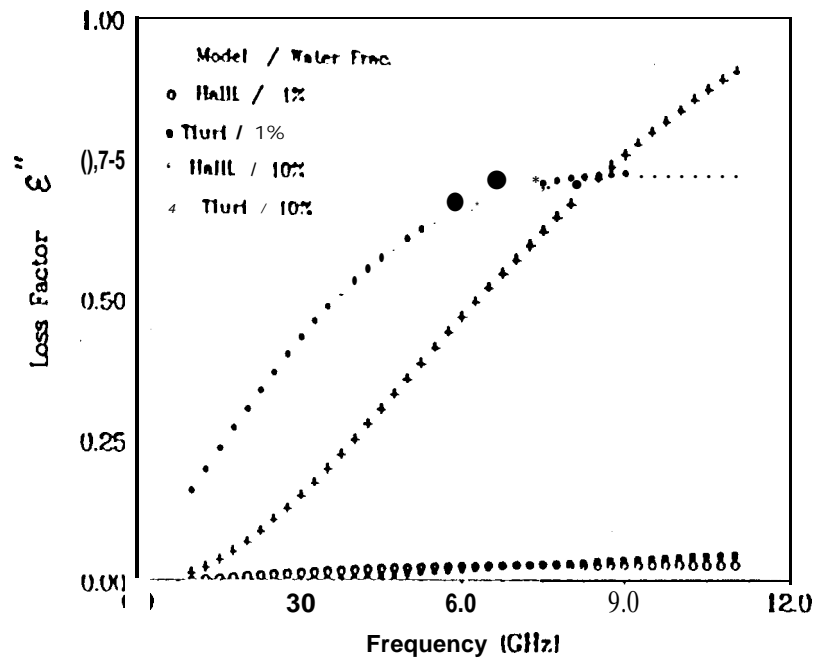
b.

Fig. 3(b) Experimental penetration depth for sea ice. computed from the values in Figure 3-7.
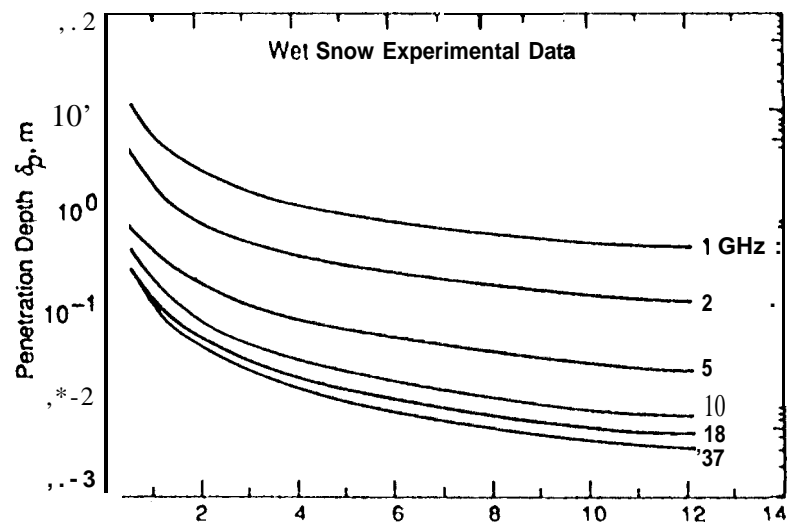
after Hallikainen and Winebrenner (1992)

a.

Wet Snow
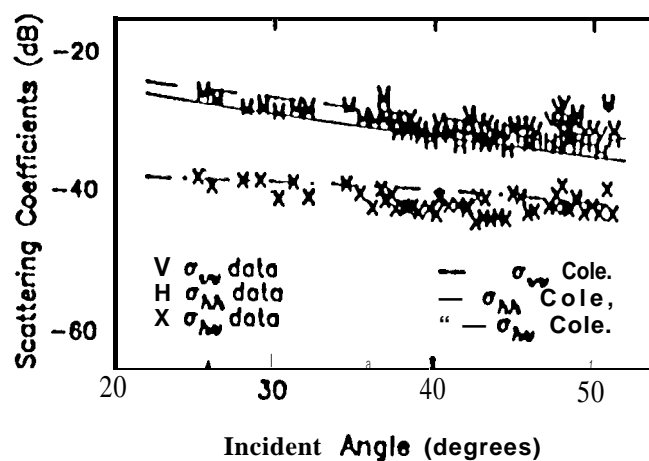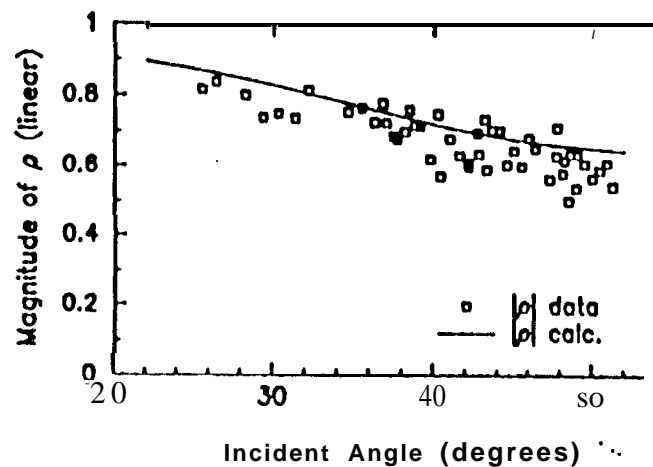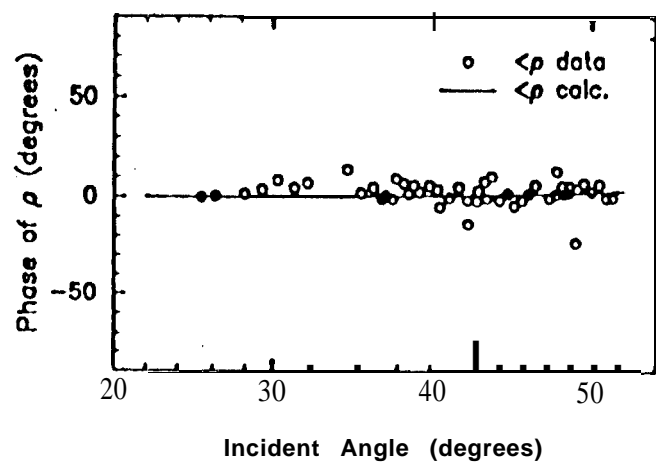
Permittivity ε'

4.00

3.00

2.00

1.00

Model / Water Frac.
○ HalIL / 1%
● Tiurl / 1%
' HalIL / 10%
+ Tiurl / 10%

0.0   3.0   8.0   9.0   12.0

Frequency (GHz)

b.

Loss Factor ε''

1.00

0.75

0.50

0.25

0.00

Model / Water Frac.
○ HalIL / 1%
● Tiurl / 1%
' HalIL / 10%
4 Tiurl / 10%

0   3.0   6.0   9.0   12.0

Frequency (GHz)

c.

Penetration Depth δ_p, m

,.2

$10'$

10^0

10^{-1}

,*-2

,.-3

Wet Snow Experimental Data

1 GHz
2
5
10
18
37

2   4   6   8   10   12   14

a.

(a) Scattering Coefficients from 1372L

Incident Angle (degrees)

(b) Magnitude of ρ from 1372L

b,

Incident Angle (degrees)

(c) Phase of ρ from 1372L
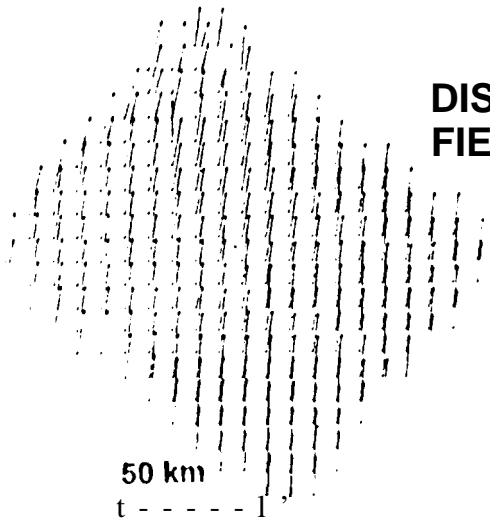
c.

Incident Angle (degrees)

FIG 4

ERS-1SAR IMAGERY
©EUROPEAN SPACE AGENCY

11-27-91
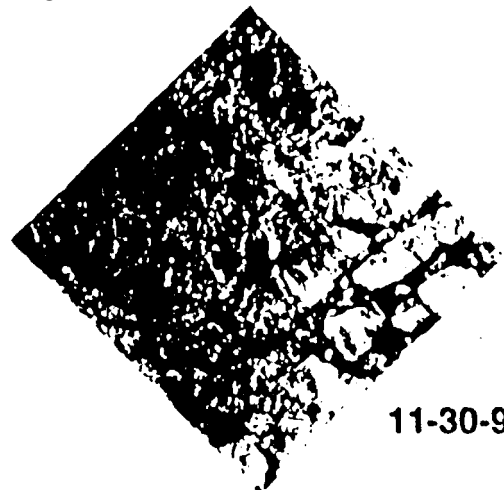
11-30-91

DISPLACEMENT FIELD
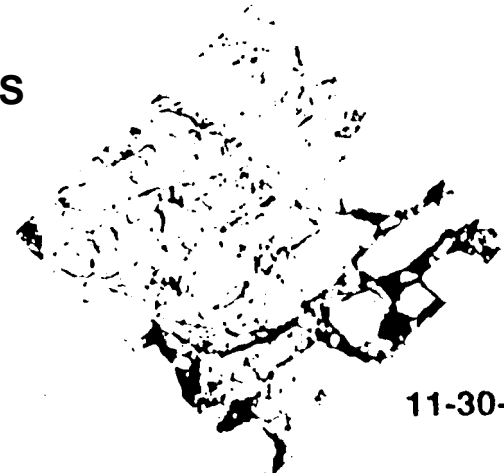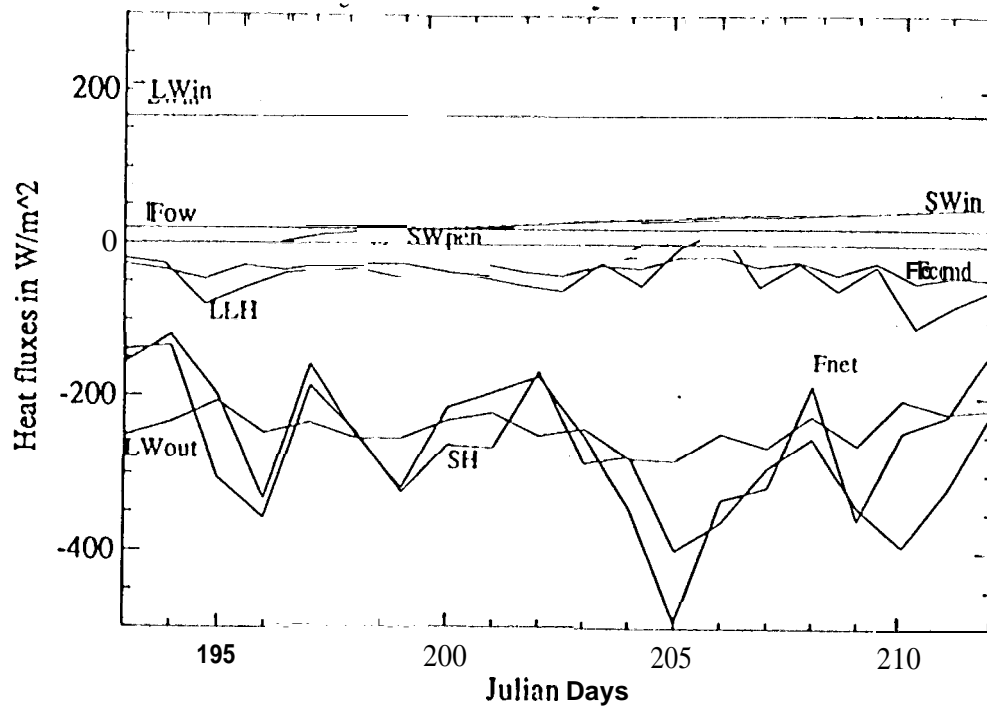
DEFORMATION GRID

50 km

ICE TYPE MAPS
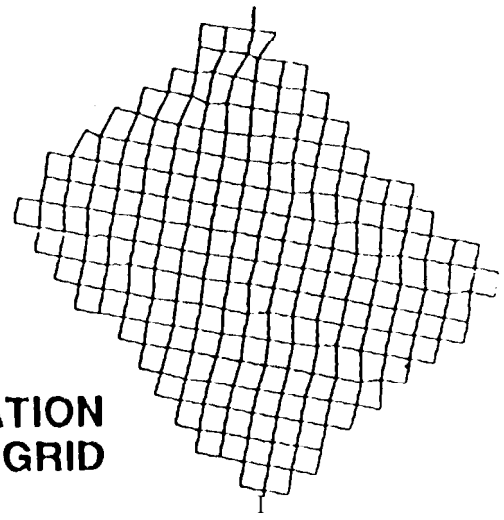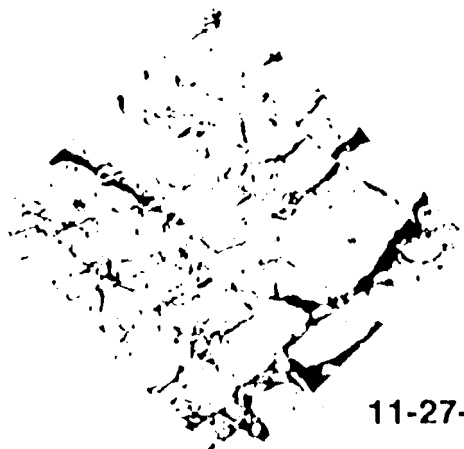
11-27-91

11-30-91
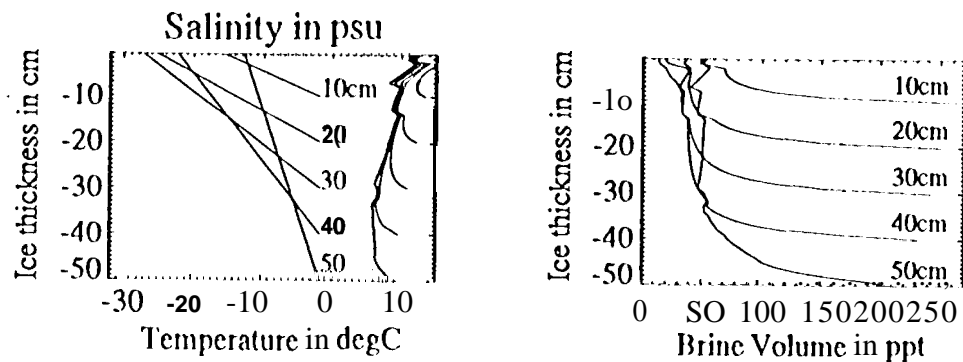
**MULTIYEAR ICE - WHITE, DEFORMED FIRST YEAR ICE - BLUE
UNDEFORMED FIRST YEAR ICE - GREEN, NEW/YOUNG ICE - RED**

FIG 5

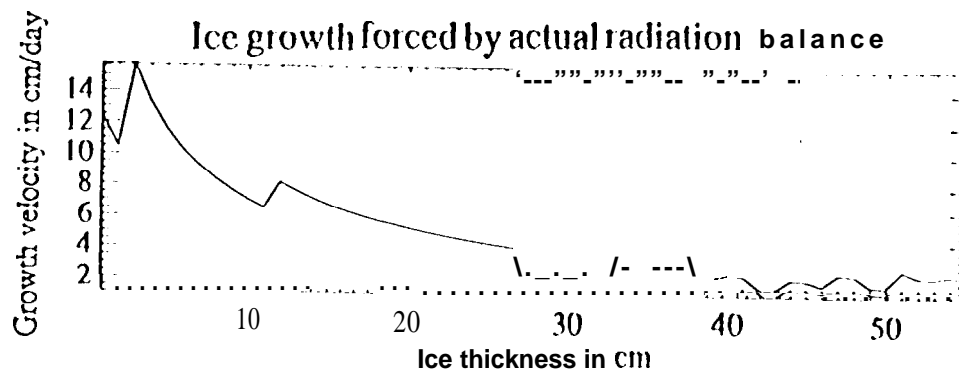FIG 6

a.

Heat fluxes in W/m^2

LWin

200

SWin

Fow

0

SWpen

Flcond

LLH

Fnet

-200

LWout

SH

-400

195   200   205   210

Julian Days

b.

Salinity in psu

Ice thickness in cm

-10   10cm
-20   20
-30   30
-40   40
-50   50

-30 -20 -10   0   10
Temperature in degC

Ice thickness in cm

-1o   10cm
-20   20cm
-30   30cm
-40   40cm
-50   50cm

0   SO 100 150200250
Brine Volume in ppt

c,

Ice growth forced by actual radiation balance

Growth velocity in cm/day

14
12
10
8
6
4
2

10   20   30   40   50
Ice thickness in cm

d.

Saltflux in kg/(m^2 month)

193.235
60
193.778
50   194.465
195.285
40   196.310
X97.876
30   200.036 202.257
20   205.719 208.8

10   20   30   40   50
Ice thickness in cm
Start Day: 193

FIG. 9